ARL-TR-7801 ● SEP 2016

US Army Research Laboratory

Planar Homojunction Gallium Nitride (GaN) P-i-N Device Evaluated for Betavoltaic Energy Conversion: Measurement and Analysis

by M Litz, W Ray, J Russo, S Kelley, and J Smith

NOTICES

Disclaimers

The findings in this report are not to be construed as an official Department of the Army position unless so designated by other authorized documents.

Citation of manufacturer's or trade names does not constitute an official endorsement or approval of the use thereof.

Destroy this report when it is no longer needed. Do not return it to the originator.

ARL-TR-7801 ● SEP 2015

US Army Research Laboratory

Planar Homojunction Gallium Nitride (GaN) P-i-N Device Evaluated for Betavoltaic Energy Conversion: Measurement and Analysis

by M Litz, W Ray, J Russo, S Kelley, and J Smith
Sensors and Electron Devices Directorate, ARL

REPORT DOCUMENTATION PAGE	Form Approved OMB No. 0704-0188

1. REPORT DATE *(DD-MM-YYYY)*	2. REPORT TYPE	3. DATES COVERED (From - To)
September 2016	Technical Report	

4. TITLE AND SUBTITLE	5a. CONTRACT NUMBER
Planar Homojunction Gallium Nitride (GaN) P-i-N Device Evaluated for Betavoltaic Energy Conversion: Measurement and Analysis	5b. GRANT NUMBER
	5c. PROGRAM ELEMENT NUMBER

6. AUTHOR(S)	5d. PROJECT NUMBER
M Litz, W Ray, J Russo, S Kelley, and J Smith	5e. TASK NUMBER
	5f. WORK UNIT NUMBER

7. PERFORMING ORGANIZATION NAME(S) AND ADDRESS(ES)	8. PERFORMING ORGANIZATION REPORT NUMBER
US Army Research Laboratory ATTN: RDRL-SED-E 2800 Powder Mill Road Adelphi, MD 20783-1138	ARL-TR-7801

9. SPONSORING/MONITORING AGENCY NAME(S) AND ADDRESS(ES)	10. SPONSOR/MONITOR'S ACRONYM(S)
	11. SPONSOR/MONITOR'S REPORT NUMBER(S)

12. DISTRIBUTION/AVAILABILITY STATEMENT

Approved for public release; distribution is unlimited.

13. SUPPLEMENTARY NOTES

14. ABSTRACT

Isotope power sources provide a continuous flow of energy from decaying isotopes. The operational lifetimes of these power sources are measured in decades, not years. The energy density of isotopes (J/kg) is 106 greater than that of chemical batteries. The energy emitted in the decay of low-energy betas from tritium (^{3}H) and nickel-63 (^{63}Ni) is converted to a trickle charge of electric current. The report describes initial measurements of energy collected in a planar homojunction gallium nitride (GaN) device. The parametric variation of electron beam energy (2.5–16 keV) enables correlation to the beta spectra of both ^{3}H and ^{63}Ni natural decay products. The analysis of the specific isotope-weighted electron beam distribution described predicts the power efficiency of the device structure as a 2-D isotope power source system. This first look at GaN device geometries suggests that optimization of device geometry in subsequent designs will employ a 3-D structure using novel growth techniques along the material crystal axis.

15. SUBJECT TERMS

gallium nitride, GaN, p-i-n, betavoltaic cell, 2-D isotope power, planar homojunction

16. SECURITY CLASSIFICATION OF:			17. LIMITATION OF ABSTRACT	18. NUMBER OF PAGES	19a. NAME OF RESPONSIBLE PERSON
a. REPORT	b. ABSTRACT	c. THIS PAGE			Johnny A Russo
Unclassified	Unclassified	Unclassified	UU	30	19b. TELEPHONE NUMBER (Include area code) 301-394-5530

Contents

List of Figures iv

List of Tables v

1. Introduction 1

2. Experimental Setup 4

2.1 Electron Beam Hardware 5

2.2 Planar GaN Device 6

2.3 Electron Beam Aperture and Alignment 8

3. Results 9

4. Conclusion 16

5. Further Evaluation 16

6. References 17

List of Symbols, Abbreviations, and Acronyms 20

Distribution List 22

List of Figures

Fig. 1 Side view of a cylindrical geometry composed of GaN p-i-n fabricated for initial energy conversion evaluations[18] 4

Fig. 2 Electron beam gun on top of the a) vacuum container containing and b) Faraday cup and translation stage for target positioning. c) Image of the entire experimental setup including the parameter analyzer, picoammeter, electron beam gun and chamber, and high-voltage cabinet. 5

Fig. 3 The GaN wafer profile using the doping profile in Khan et al.[21] 6

Fig. 4 Image of fabricated GaN device inside 40-pin dual inline package (DIP). The red circles identify the 2 devices tested (28 and 33). Device 28 p-layer diameter is 620 µm and total diameter is 773 µm, including metal ring contacts. Device 33 p-layer diameter is 844 µm and total diameter is 958 µm, including metal ring contacts. 7

Fig. 5 Electrical schematic for the measurement of the betavoltaic cell.....7

Fig. 6 Device testing stage with translation stages, electrical connections, and phosphor-lined pinhole aperture 8

Fig. 7 a) Image of phosphor-lined pinhole aperture irradiated by electron beam. This identifies the location and approximated the total current through aperture. b) Illustration of pinhole aperture attached to moveable stage inside vacuum chamber. c) Image of aperture covered device inside 40-pin DIP before being loaded in chamber. 9

Fig. 8 GaN device dark (leakage) current plots for Devices 28 and 33. Clearly, Device 33's dark current cannot be used for betavoltaic applications since the leakage current is higher than output current response when irradiated by electron beam. Device 28's signal is noisy but adequate for testing. The leakage current is in the pico-amperes, which is lower than the output current response during irradiation.....10

Fig. 9 a) The current and voltage for the GaN device was measured on an HP parameter analyzer HP4155B. b) The maximum power output is calculated in order to evaluate device efficiency and apply weighted beta-decay spectra simulating ^{3}H and ^{63}Ni. The MPP plot does not include weighted percentage to beta-decay spectra to ^{3}H or ^{63}Ni.....11

Fig 10. Device 28 power efficiency as function of electron energy is shown. The maximum efficiency is at 11.25 keV. The 2 red solid lines distinguish 2 regions of the device's nonlinear response. The inflection point represents the threshold of penetration depth in depletion region when the electron energy is greater than 11.25 keV. 12

Fig 11. The zero-bias electric field of the device. The field variation is biggest at the p-n junction, with a small electric field built at the junction between the intrinsic and n+ regions.[22].....14

Fig. 12 The energy deposited in successive 100-nm layers of GaN is shown as a function of the energy of the monoenergetic electron beam irradiating the GaN device. A 5-keV electron beam will deposit most energy into the first 100 nm. A 12-keV electron beam will deposit most of its energy into the 400-nm layer. 14

Fig. 13 Intensity as function of energy for ^{3}H and ^{63}Ni beta spectrum is shown. The intensities are normalized for each beta spectrum. Output power density and power conversion efficiency are weighted by multiplying the normalized intensities and summation. 15

List of Tables

Table 1 The energy efficiency (η) of GaN-based betavoltaic cells shows limited progress with 2-D (planar) devices.....3

Table 2 Device 28 electrical parameters as a function of electron energy. Maximum open-circuit voltage and power conversion efficiency are at 12.5 keV. As electron energy increases, FF increases and then saturates at 12.5 keV. 13

INTENTIONALLY LEFT BLANK.

1. Introduction

The work described in this interim report is motivated by the challenge to develop efficient energy-conversion techniques, starting with decaying isotopes and ending in electrical current flow for power sources. Both direct energy conversion (DEC) and indirect energy conversion (IDEC) experimental platforms are being developed to understand the interactions of high-energy electrons with semiconductor materials and phosphors.[1] Betavoltaic cells are DEC systems and, generally, are more efficient than IDEC systems using tritium (^{3}H) and nickel-63 (^{63}Ni). Beta-photovoltaic cells are IDEC systems. Their power efficiency is limited by the conversion efficiency of the scintillator, such as a phosphor, the energy median between the beta source and photovoltaic cell.

Wide bandgap (E_g) materials such as silicon carbide (SiC)/4H-SiC and gallium nitride (GaN) are known to have a higher energy conversion efficiency limit than silicon (Si) and gallium phosphide betavoltaics. This is, in part, through an increase of the open-circuit voltage and a reduction in the short-circuit current. The high on-state voltage matches with electrical circuit voltage requirements, leading to smaller DC/DC converter conversion ratios and thereby increasing conversion efficiency. The low on-state current also has a benefit of reducing the resistive losses that can occur. However, due to the lower current generation, losses due to parasitic shunt resistance are non-negligible. Device fabrication, structure design, and packaging with strict quality requirements are needed to improve the ability of the betavoltaic to produce energy above the shunt resistance. The fabrication of SiC and GaN semiconductors has been plagued by the presence of defects within the semiconductor material, reducing their efficiency. It is not until recently that wafer quality of SiC has been improved due to wider use in power components application.

SiC betavoltaic cells were the first wide bandgap semiconductor to be commercially available as a betavoltaic battery.[2] This was due to the development of mass-production semiconductor processing methods of 4H-SiC. The ease of fabrication of thicker epitaxial layers make SiC a prime material for the use of betavoltaic cells. SiC is an attractive material due to its indirect bandgap, which can lead to better recombination time within the semiconductor. Longer recombination times can directly increase the diffusion collection of the semiconductor material. The published research of SiC as a betavoltaic cell has yielded problems for increasing efficiency past 6% when used with a beta isotopes such as ^{63}Ni.[3–5] Widetronix Inc., has developed a betavoltaic cell using titanium tritide ($Ti^{3}H_x$) metal foil as the beta source and 4H-SiC (E_g = 3.23–3.26 eV) as the semiconductor. The betavoltaic cell

has a power efficiency greater than 18% with an input power of approximately 0.7 $\mu W/cm^2$ (14.92 mCi/cm^2) from one side.[6]

GaN has a higher estimated material efficiency for betavoltaic conversion than SiC due to an 8% larger bandgap. Klein et al. formed this limiting efficiency based on the characteristics of the material, using an ideal betavoltaic conversion device.[7] Using Klein's Equation, the upper limit for GaN betavoltaic conversion at room temperature is 34%, which is above 4H-SiC.[7] Olsen et al. provided calculated limiting efficiencies that included the source efficiency when using a foil-backed-based source.[8] These examinations show how the ultimate efficiency for betavoltaic materials has yet to be empirically shown. One limiting efficiency that has yet to be demonstrated is the energy conversion efficiency of the material as an energy-generating semiconductor device. All betavoltaic devices have parasitic resistances that reduce their energy-providing capability that are inherent to the material.

Overcoming the leakage current in materials is a challenge in low-isotope-activity betavoltaic devices. The betavoltaic device must generate a current orders of magnitude higher than the leakage current to minimize losses. However, higher generation current is directly countered by parasitic series resistance. The parasitic series resistance is composed of elements such as resistance due to the metal contacts, the device structure dimensions, and the material parameters. These parameters, such as charge carrier mobility and carrier concentration, are extremely important to forming an estimate on limiting efficiency that involves semiconductor physics. If the Klein Equation graph[7] is to be believed, Si would be the most practical betavoltaic device, because it is the most developed semiconductor device. That being said, a homojunction Si semiconductor is not radiation tolerant and has a low open-circuit voltage compared to previously mentioned wide bandgap devices.

GaN semiconductor devices offer the ability to increase the capability of betavoltaic direct energy converters due to GaN's higher bandgap energy,[9] radiation hardness,[10] and intrinsic carrier concentration.[11] Radiation damage on GaN devices were investigated from 2001 to 2005 for both proton-induced damage[12] and cobalt-60 (^{60}Co) gamma ray-induced damage.[12–15] These early measurements verified the radiation tolerance of GaN devices, both Schottky[14] and p-i-n.[13,15] GaN has a radiation threshold energy of 440 keV for electron irradiation, which is much higher than the spectrums of ^{63}Ni and ^{3}H. GaN devices have been developed for betavoltaic power sources in both bulk and thin-film devices. Refer to Table 1 for reported GaN betavoltaic cell energy efficiencies. The long-life capability of a wide bandgap GaN with enhanced energy conversion through modified doping profiles in n-type material layer has been shown.[9] GaN's lower intrinsic carrier

concentration means there is less space-charge current within the device, allowing for higher current generation when acting as a SiC or Si betavoltaic. Even though GaN is not a well-understood material, the direct wide bandgap and electrical properties make it a suitable power semiconductor and betavoltaic converter. GaN has higher charge carrier mobility, breakdown field, and intrinsic carrier concentration than 4H-SiC.

Table 1 The energy efficiency (η) of GaN-based betavoltaic cells shows limited progress with 2-D (planar) devices

Year	Device structure	Source	η (%)	Reference(s)
2010	P-i-N	^{63}Ni	0.004	Cheng et al.[17]
2011	Schottky	^{63}Ni	0.32	Lu et al.[23]
2011	P-i-N	^{63}Ni	1.13	Cheng et al.[24]
2011	P-i-N	^{63}Ni	1.60	Lu et al.[11]
2011	PiN	^{63}Ni	1.80	Cheng et al.[25], Tang et al.[26]
2012	Sandwiched PN	^{147}Pm	13.40*	San et al.[27]
2013	Schottky	^{63}Ni	2.25*	Wang et al.[19]
2014	P-i-N	^{147}Pm	0.44	Liu et al.[28]
2015	P-i-N	^{63}Ni	0.29	Munson et al.[29]
2015	P-i-N	^{63}Ni	2.91	Li et al.[16]

*indicates simulated results
Note: ^{147}Pm = promethium 147

Limitations in power conversion efficiency reaching the "Klein efficiency" are observed because of defects in fabrication and formation of dead layers at interface.[16] Thick GaN layers form cracks due to lattice mismatch during growth on foreign substrates such as sapphire (Al_2O_3). Previous publications have shown that the width of the depletion region of GaN p-n junction is too narrow, less than 1 micron, to efficiently collect radiation-generated electron-hole pairs (EHPs), especially for higher energy beta-emitters like nickel-63 (^{63}Ni) and promethium-147 (^{147}Pm). The beta particle penetration depth in bulk GaN is approximately 1.8 µm for ^{63}Ni (E_{avg} = 17 keV) and 300 nm for ^{3}H (E_{avg} = 5.7 keV).[17] Monte Carlo n-particle extended (MCNPX) modeling of energy deposition in GaN suggests that the depletion region should be 150–700 nm thick for ^{3}H source in order to enclose greater than 68% of the generated free carriers.[18] Figure 1 shows the structure of GaN modelled and used in experiments. For ^{63}Ni and ^{147}Pm, the depletion region would need to 3 and 12 times thicker, respectively.

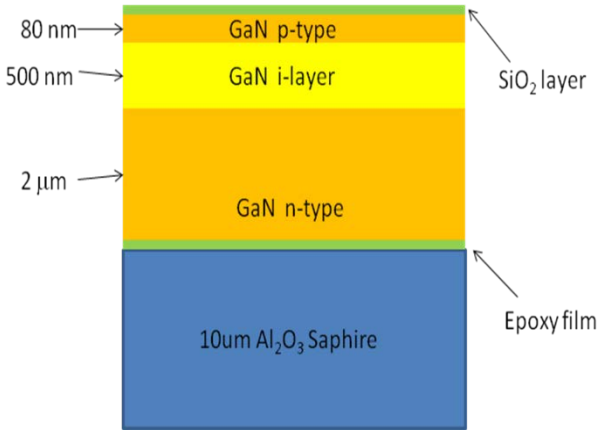

Fig. 1 Side view of a cylindrical geometry composed of GaN p-i-n fabricated for initial energy conversion evaluations[18]

The depletion region, also called the intrinsic or undoped layer, is limited by the dopant concentration (holes and electrons). In order to improve the power conversion efficiency of a planar (2-D) GaN betavoltaic cell, the thickness of the depletion layer must be maximized to collect the highest number of generated electron-hole pairs (EHPs). Geometry beyond 2-D layering enhances the interaction space increasing device efficiency. As such, 3-D structures are expected to greatly enhance the device efficiency and enable higher output power on the same wafer footprint. GaN material fabrication processes are under research to improve the quality of GaN. In conclusion, GaN devices with high-quality material offer a direct improvement over SiC devices.

This report analyzes the power efficiency of a single homojunction GaN device during electron beam irradiation from a flood gun. Electron energy ranges from 2.5 to 16 keV with a fixed beam size irradiated the device. The current-voltage (I-V) curve is measured for each electron energy. Parametric variation of incident energy of stimulating electrons and weighting factors are used to simulate β-spectra from ^{3}H and ^{63}Ni. A process for analyzing voltage and current data obtained on a single GaN device structures is described.

2. Experimental Setup

The measurements described in this report are useful in simulating the beta spectra of ^{3}H and ^{63}Ni. These 2 isotopes are commercially available isotopes with low bio-toxicity and relatively low-energy β emission. Another isotope often described in the literature for isotope power source applications is ^{147}Pm.[19] The total energy liberated in each decay is always the endpoint energy (18.6, 67, and 225 keV respectively).[20] The integrated value under the beta spectrum for ^{3}H, ^{63}Ni, and

^{147}Pm (5.7, 17.4, and 62 keV, respectively) is the average energy released in each decay, because antineutrinos are always released along with β particles due to conservation laws.

2.1 Electron Beam Hardware

The system uses a Kimball Physics EMG-12 electron gun, capable of supplying a monoenergetic electron beam with currents up to 500 μA and energies ranging from 0 to 16 kV. The EMG-12 heats a tantalum disc with a tungsten filament to achieve thermionic emission. The electron spot size is adjustable from 0.5 mm to 1 cm using the grid and focus setting knobs. The beam is transported 8 inches in a 6-inch-diameter vacuum chamber. The vacuum chamber supporting the electron gun, Faraday current measuring device, and target translation stage is shown in Fig. 2.

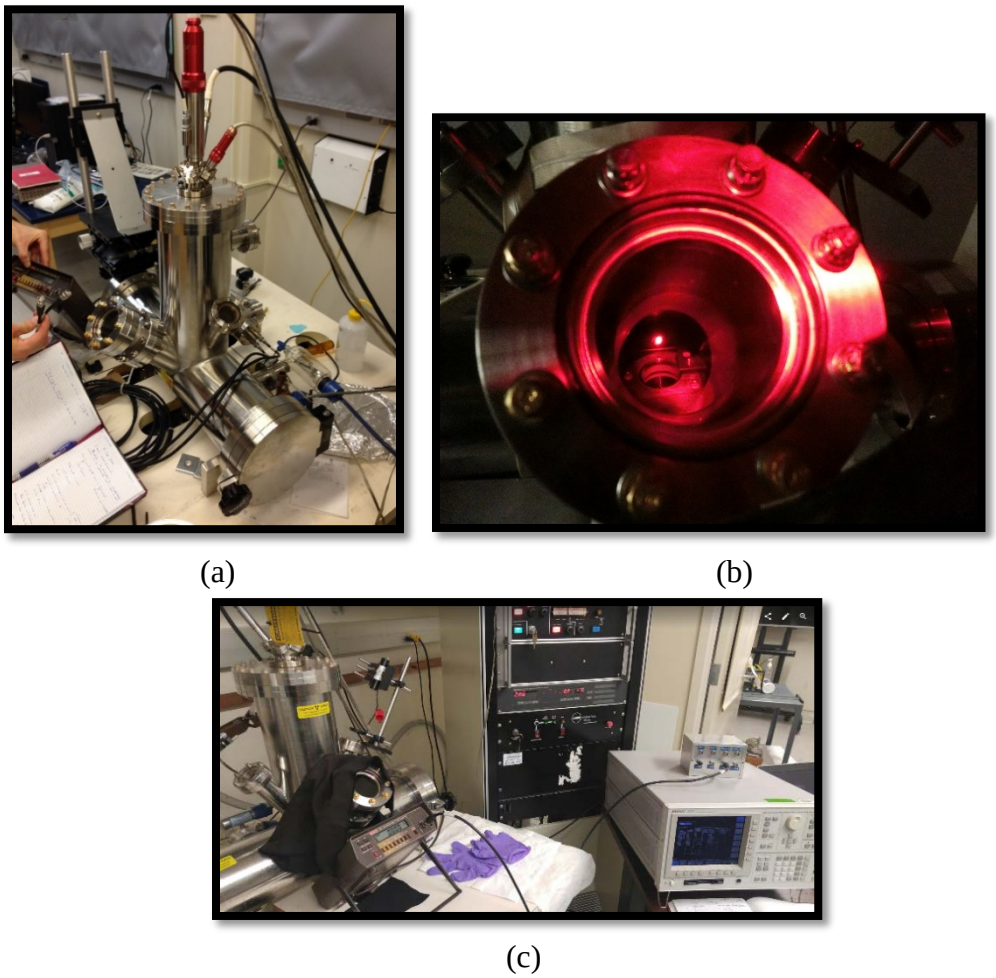

(a) (b)

(c)

Fig. 2 Electron beam gun on top of the a) vacuum container containing and b) Faraday cup and translation stage for target positioning. c) Image of the entire experimental setup including the parameter analyzer, picoammeter, electron beam gun and chamber, and high-voltage cabinet.

A pair of Newport Agilis series linear stages provide in-vacuum x-y translation of the sample. I-V data are measured using a Hewlett-Packard (HP) 4155B parameter analyzer. To measure the beam current on target, we use a Keithley 485 picoammeter with a Faraday cup. The sample is loaded into the chamber, which is then pumped down to 2×10^{-6} Torr before the electron gun is powered on. For a more stable beam current during measurement, the electron gun is warmed up for 45 min to allow the temperature of the filament to stabilize. The desired accelerating voltage and beam current are then set. Typically, we keep current constant at 0.1–1 nA while varying the voltage for each measurement from 2 to 16 keV. The electron beam current can be set as high as 1 mA; however, the 0.1- and 1-nA current settings are very stable and represent the low intensity expected from radioisotope beta decay.

2.2 Planar GaN Device

The GaN wafer was grown on a 2-inch Al_2O_3 substrate by our collaborator State University of New York Albany using a Veeco D180 metalorganic chemical vapor deposition (MOCVD) reactor. Refer to Fig. 3 for the GaN wafer profile. GaN dopant values and fabrication process are explained in detail in Khan et al.[21] The wafer was fabricated at the US Army Research Laboratory, Adelphi, Maryland. For p-type contacts, titanium (Ti) (500 Å)/gold (Au) (1,500 Å) is deposited using electron beam deposition. The mesas are etched in an ULVAC NE-550e high-density plasma etcher. Ti (250 Å)/aluminum (Al) (2,200 Å)/nickel (Ni) (600 Å/ Au (500 Å) was then deposited for n-type contacts using e-beam deposition. Both the p- and n-type contacts are annealed at 500 °C in nitrogen gas ambient.

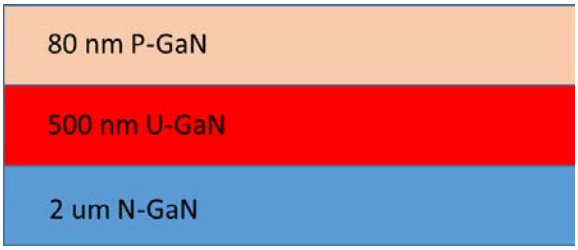

Fig. 3 The GaN wafer profile using the doping profile in Khan et al.[21]

Figure 4 shows an image of the wafer after fabricated and device sizes for 28 and 33, which are the tested devices. Wafer and device images are taken using a Leica optical microscope; refer to Fig. 4. The same microscope was used to center the electron beam aperture over the GaN device.

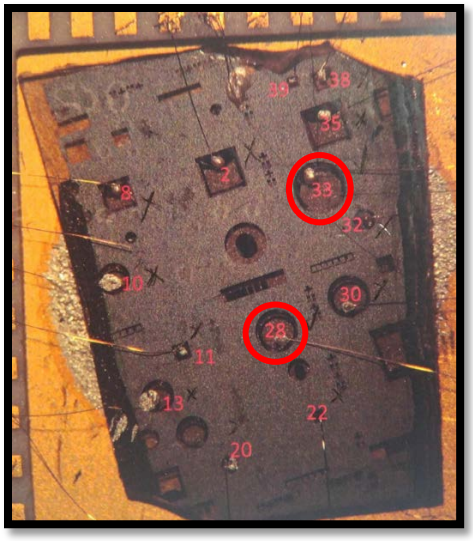

Fig. 4 Image of fabricated GaN device inside 40-pin dual inline package (DIP). The red circles identify the 2 devices tested (28 and 33). Device 28 p-layer diameter is 620 µm and total diameter is 773 µm, including metal ring contacts. Device 33 p-layer diameter is 844 µm and total diameter is 958 µm, including metal ring contacts.

Devices 28 and 33 were selected for electron beam irradiation measurement. The current and voltage for each device was measured on HP 4155B parameter analyzer during electron beam (e-beam) exposure. The devices under testing were placed on the translation stage inside the vacuum chamber and wire bonded to the internal package connections. The package connection wires lead to vacuum rated connections (~2 inches) and continue to the parameter analyzer (~4 inches). The connections of the schematic are shown in Fig. 5.

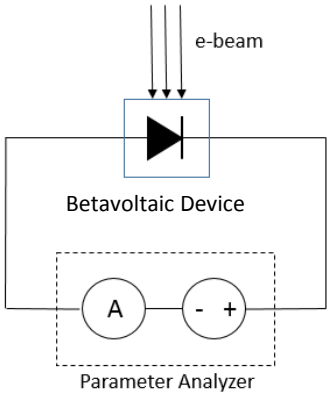

Fig. 5 Electrical schematic for the measurement of the betavoltaic cell

2.3 Electron Beam Aperture and Alignment

The etching pit density GaN package (EPD GaN01) was placed in a 3-D-printed, 40-pin package holder attached to a copper (Cu) board. The Cu board was screwed down to an x-y translation stage. A single device was connected to the parameter analyzer through the vacuum chamber (Fig. 6).

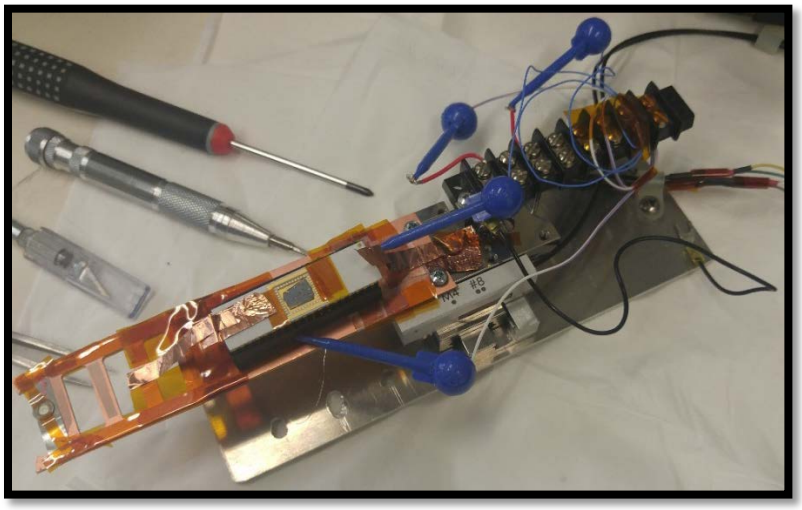

Fig. 6 Device testing stage with translation stages, electrical connections, and phosphor-lined pinhole aperture

The electron beam location was determined using a zinc sulfide (ZnS):Cu,Al phosphor. The phosphor was then marked with a helium-neon laser through chamber's optical port window. A stainless steel foil aperture ($\emptyset \approx 560\ \mu m$) was attached to the end of the FR4 board. The ZnS:Cu,Al phosphor was placed around the hole as a visual electron beam marker. The stages move the aperture overtop of the Faraday cup, which was kept stationary underneath the electron beam. Approximately 0.10 nA (100 pA ± 4 pA) was measured by the Faraday cup through the aperture giving a current density of almost equal to 40 nA/cm^2. The stages move for electron beam centering; centering motion stops once maximum current is measured using the Keithley 485 Autoranging picoammeter (error = 0.4%, resolution = 0.1 pA, 100 pA ± 4.4 pA). Between each measurement, the accelerating voltage was changed and the current was kept constant. Another aperture of the same size is placed over the device with ZnS:Cu,Al on the surface. Both metal apertures are grounded to prevent electric charge buildup. Results of parametric studies of applied voltage from 2.5 to 16 keV on GaN device follow. Figure 7 shows images and illustrations of the aperture setup. The sample was diced to fit into a standard 40-pin DIP.

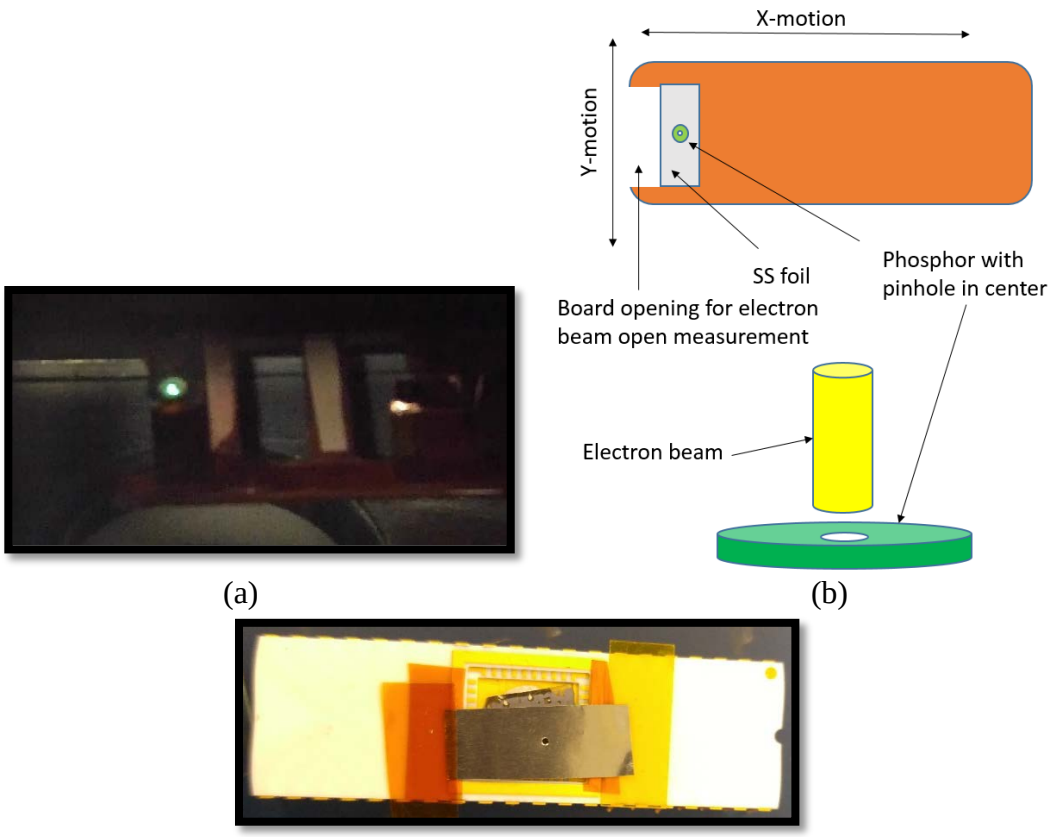

Fig. 7 a) Image of phosphor-lined pinhole aperture irradiated by electron beam. This identifies the location and approximated the total current through aperture. b) Illustration of pinhole aperture attached to moveable stage inside vacuum chamber. c) Image of aperture covered device inside 40-pin DIP before being loaded in chamber.

3. Results

Two devices (28 and 33) on the EPD GaN01 wafer were examined. Before electron beam irradiation, dark current (leakage current) was measured for each device (Fig. 8). Device 28 was the only device that showed characteristics of ideal diode behavior relative to leakage current. Device 33 leakage current was too high, preventing us from measuring output current during electron beam irradiation. All I-V curves are measured on an HP parameter analyzer 4155B.

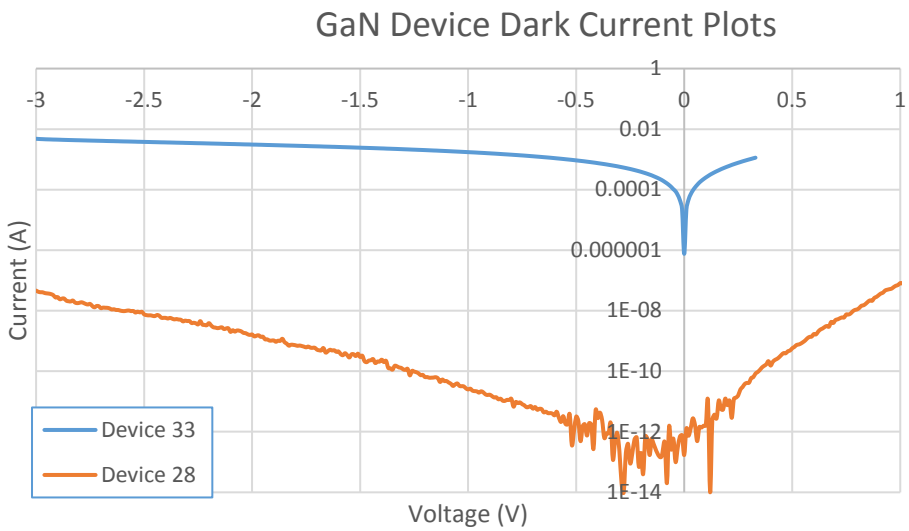

Fig. 8 GaN device dark (leakage) current plots for Devices 28 and 33. Clearly, Device 33's dark current cannot be used for betavoltaic applications since the leakage current is higher than output current response when irradiated by electron beam. Device 28's signal is noisy but adequate for testing. The leakage current is in the pico-amperes, which is lower than the output current response during irradiation.

Only Device 28 from the EPD GaN01 wafer was irradiated by the electron beam during the experiment. Electron beam energy was varied over the range of 2.5–16 keV (maximum input electron energy emission) while the total current through aperture was maintained at almost equal to 0.10 nA. The resulting set of I-V curves are shown in Fig. 9. The maximum power point (MPP) was calculated for each applied voltage.

(a)

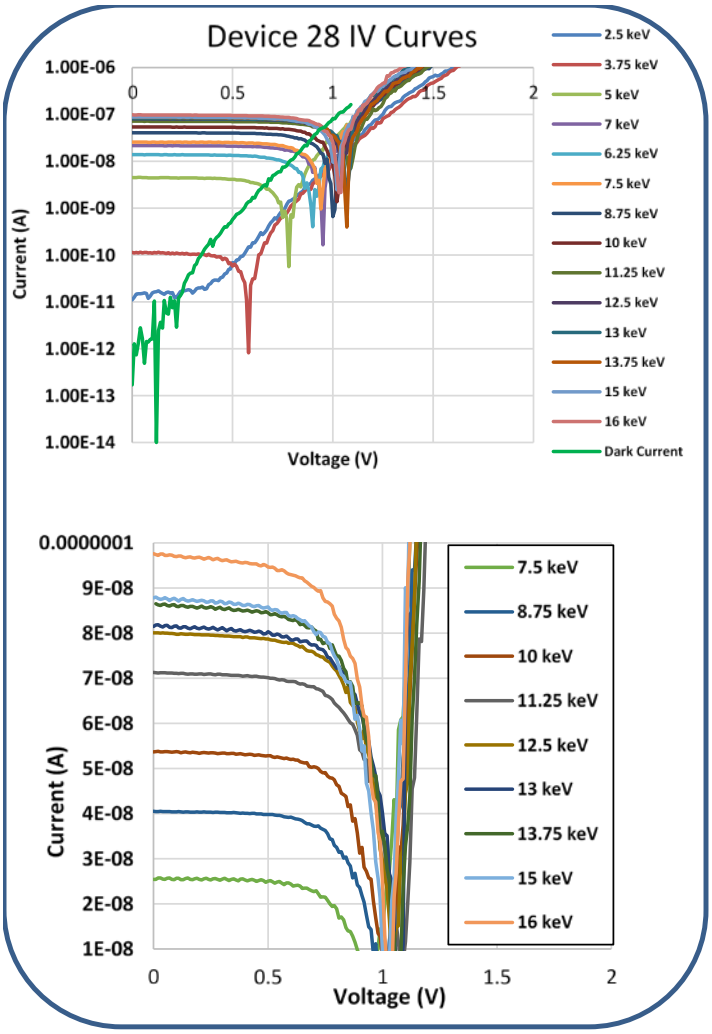

(b)

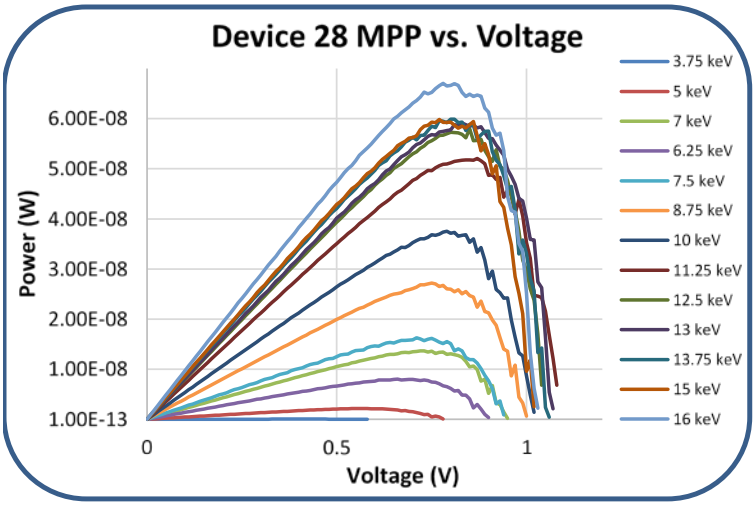

Fig. 9 a) The current and voltage for the GaN device was measured on an HP parameter analyzer HP4155B. b) The maximum power output is calculated in order to evaluate device efficiency and apply weighted beta-decay spectra simulating ^{3}H and ^{63}Ni. The MPP plot does not include weighted percentage to beta-decay spectra to ^{3}H or ^{63}Ni.

From the I-V curves shown in Fig. 9, the open-circuit voltage (V_{oc}) and short-circuit current density (J_{sc}) can be identified. The product of measured I and V was determined (see Fig. 9b) within the HP4155 parameter analyzer showing the voltage position. Power conversion efficiency was calculated using the device output power density (W_e/cm^2) over input power density (W/cm^2) from the electron beam. Figure 10 shows a device power efficiency as a function of electron energy (E_e). Table 2 displays short-circuit current (I_{sc}), open-circuit voltage (V_{oc}), fill factor (FF), output power density (S_e), and power efficiency (η).

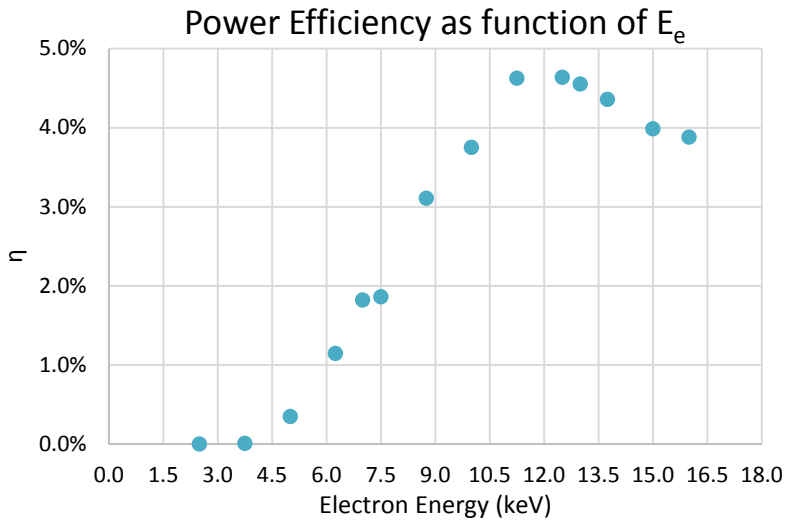

Fig 10. Device 28 power efficiency as function of electron energy is shown. The maximum efficiency is at 11.25 keV. The 2 red solid lines distinguish 2 regions of the device's nonlinear response. The inflection point represents the threshold of penetration depth in depletion region when the electron energy is greater than 11.25 keV.

Table 2 Device 28 electrical parameters as a function of electron energy. Maximum open-circuit voltage and power conversion efficiency are at 12.5 keV. As electron energy increases, FF increases and then saturates at 12.5 keV.

E_e (keV)	I_{sc} (A)	V_{oc} (V)	S_e (W_e/cm^2)	FF	η
2.5	0	0	0	0	0.000%
3.75	1.1374E-10	0.58	4.03568E-11	61%	0.01%
5	4.48757E-09	0.78	2.17745E-09	62%	0.35%
6.25	1.38638E-08	0.9	8.00897E-09	64%	1.14%
7	2.15038E-08	0.95	1.36619E-08	67%	1.82%
7.5	2.54531E-08	0.94	1.62764E-08	68%	1.86%
8.75	4.05012E-08	1.01	2.7202E-08	66%	3.11%
10	5.36442E-08	1.02	3.75251E-08	69%	3.75%
11.25	7.13112E-08	1.09	5.20E-08	67%	4.62%
12.5	8.00539E-08	1.10	5.79697E-08	70%	4.64%
13	8.14591E-08	1.07	5.91621E-08	68%	4.55%
13.75	8.65194E-08	1.06	5.99069E-08	65%	4.36%
15	8.77651E-08	1.02	5.98166E-08	67%	3.99%
16	9.76164E-08	1.03	6.70551E-08	67%	3.88%

Figure 11 shows a device simulation for a GaN device with a similar doping profile as compared to the experimental device. The figure shows the electric field of an unbiased device, which corresponds to the depletion region. The depletion region shows that only a portion of the deposited energy within the device is actually able to transport from the device as generated electricity.[22] The energy deposition profiles within the GaN device are consistent with the depletion region area as calculated from MCNPX modeling of bulk GaN devices.[18] Figure 12 shows the energy deposited in 100-nm layers of GaN from monoenergetic electron beams with respect to the input particle energy. As shown, the maximum energy deposited within the first 4 layers came from 12-keV electrons. This is consistent with the Silvaco ATLAS device simulation as performed by Ray et al.[22]

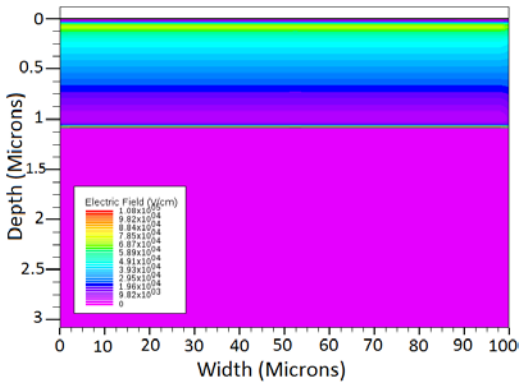

Fig 11. The zero-bias electric field of the device. The field variation is biggest at the p-n junction, with a small electric field built at the junction between the intrinsic and n+ regions.[22]

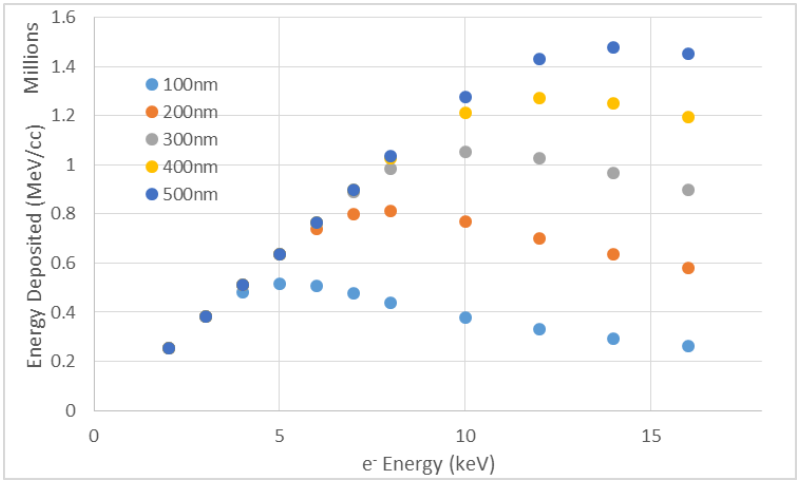

Fig. 12 The energy deposited in successive 100-nm layers of GaN is shown as a function of the energy of the monoenergetic electron beam irradiating the GaN device. A 5-keV electron beam will deposit most energy into the first 100 nm. A 12-keV electron beam will deposit most of its energy into the 400-nm layer.

The maximum measured open-circuit voltage was 1.10 V at 12.5 keV. The maximum calculated power efficiency and FF from measured results was at 12.5 keV. The visual description of FF was the ratio of the actual maximum obtainable power to the product of the open-circuit voltage and short-circuit current. The difficulty in measuring the details of reflectance efficiency, thermodynamic efficiency, charge carrier separation efficiency and conductive efficiency makes FF a useful parameter in evaluating performance. As a reference value, typical commercial solar cells had a FF of greater than 0.7. Cells with a high FF have a low series resistance and a high shunt resistance, R_{sh}. The high R_{sh} is essential for low current devices to be useful, so less of the current produced by the cell is dissipated in internal losses.

The nonlinear response of the device power efficiency and MPP (and eventual reduction of power output) with kinetic energy of the electron beam is indicative of the limited depth of the device energy conversion. The nonlinear response can be divided into 2 distinct regions of power generation (Fig. 10). The first occurs during lower energy electron stimulation (<11.25 keV). The electrons deposit all their energy in the volume of the device where charge collection can occur (depletion region). The second regime is for electron energies (>11.25 keV), where EHP creation takes place beyond the depletion region. Higher energy electrons increase the energy deposited, but less of it is available to be collected and converted into electrical current output. The 2 distinct regions of power generation as a function of input electron energy emphasize the fact that when the energy deposition range exceeds that of the depletion region, the device is no longer as efficient at collecting the charge generated in EHP creation.

MPP and power efficiency at monoenergetic electron energies is weighted to beta spectra of ^{3}H and ^{63}Ni. Figure 13 shows a plot of ^{3}H and ^{63}Ni spectrum used to weight the beta energy. The electron beam encompasses 99.89% of the ^{3}H beta energy spectrum and 62.13% of the ^{63}Ni beta energy spectrum. The ^{3}H weighted efficiency and power density are 1.28% and 2.82 $\mu W_e/cm^2$. For 62.13% of the ^{63}Ni energy spectrum, the weighted efficiency and power density are 0.045% and 0.074 $\mu W_e/cm^2$. The enormous difference between weighted efficiencies is not surprising since a larger percentage of energy from ^{63}Ni propagates through the depletion region, limiting EHP creation. The weighted device efficiencies are assuming linear response, independent of source current density (either beta or high electron energy source).

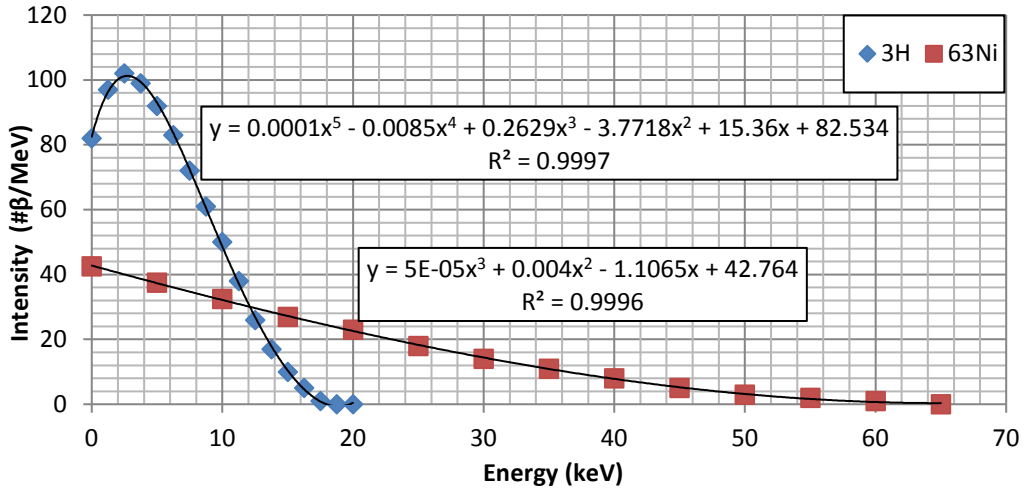

Fig. 13 Intensity as function of energy for ^{3}H and ^{63}Ni beta spectrum is shown. The intensities are normalized for each beta spectrum. Output power density and power conversion efficiency are weighted by multiplying the normalized intensities and summation.

4. Conclusion

A betavoltaic experimental platform has been developed to reliably measure the semiconductor characteristics, such as power conversion efficiency, and evaluate the efficiency of these devices in simulated ^{3}H and ^{63}Ni environments (99.89% and 62.13% of the beta energy spectrum), along with proposing new structures that will improve conversion efficiency and power density. Weighting the input power of electron source and device power efficiency gives us a value of 1.28% and 0.045% for ^{3}H and ^{63}Ni. However, semiconductor device current density linear response has not been measured yet. We plan to fabricate similar device structures in GaN with particular attention to variation of the intrinsic/depletion (undoped) region thickness. It is expected, based on electron beam energy deposition calculations in GaN, that the power out and device efficiency will increase until the thickness exceed 2 μm and 700 nm when using ^{63}Ni and ^{3}H sources.

5. Further Evaluation

Modeling using MCNPX and Silvaco ATLAS will be performed to identify an optimal GaN structure layout for the next set of measurements. The GaN simulation model developed can be used to verify the fundamental material characteristics of the GaN and optimize power conversion efficiency for planar devices (2-D). After continuity is reached between the 2-D model and experimental results, a 3-D model will be developed to design a high aspect ratio device. This increase in surface area will increase the interaction between the beta source and semiconductor converter, thus increasing energy density.

6. References

1. Bower KE, Barbanel YA, Shreter YG. Polymers, phosphors, and voltaics for radioisotope microbatteries. Boca Raton (FL): CRC Press; 2002.

2. Chandrashekhar M, Thomas C, Li H, Spencer M, Lal A. Demonstration of a 4H-SiC betavoltaic cell. Mat Sci Forum. 2006;527–529:1351–1354.

3. Da-Yong Q, Wei-Zheng Y, Peng G, Xian-Wang Y, Bo Z, Lin Z, Hui G, Hong-Jian Z. Demonstration of a 4H-SiC betavoltaic nuclear battery based on schottky barrier diode. Chinese Phys Let. 2008;25(10):3798–3800.

4. Guo H, Shi Y, Zhang Y, Zhang Y, Han J. Fabrication of SiC p-i-n betavoltaic cell with 63Ni irradiation source. In: 2011 IEEE International Conference of Electron Devices and Solid-State Circuits, 2011.

5. Levinshtein M, Rumyantsey S, Shur M. Properties of advanced semiconductor materials. New York (NY): Wiley; 2001.

6. Thomas C, Portnoff S, Spencer MG. High efficiency 4H-SiC betavoltaic power sources using tritium radioisotope. Appl Phys Let. 2016;108.

7. Klein C. Bandgap dependence and related features of radiation ionization energies in semiconductors. J Appl Phys. 1968;39(4):2029.

8. Olsen LC. Review of betavoltaic energy conversion. NASA White Paper, Washingtion State University, Richland, WA; 1993.

9. Xiao Bin T, Yun Peng L, Ding, Da C. Optimization design of GaN betavoltaic microbattery. Science China Tech Sci. 2012 Mar;55(3).

10. Wang G-q, Yang, Liu. Electrical performance of GaN diode as betavoltaic isotope battery energy converter. Atomic Energy Sci and Tech. 2013;47(12):2365–2369.

11. Lu M, Wang G, Yao C. Gallium Nitride for nuclear batteries. Advanced Mat Research Vols. 2012;343–344:56–61.

12. Emtsev VV. Radiation-induced defects in n-type GaN and InN. Physica B. 2001;308–310:51–61.

13. Umana-Membreno GA, Dell JM, Hessler TP, Nener BD, Parish G, Faraone L. 60Co gamma-irradiation-induced defects in n-GaN. Appl Phys Let. 2002;80(23).

14. Umana-Membreno GA, Dell JM, Parish G, Nener BD, Faraone L, Mishra UK. 60Co gamma irradiation effects on n-GaN schottky diodes. IEEE Trans Electron Dev. 2003 Dec;50(12).

15. Honsberg C, Doolittle WA, Allen M, Wang C. GaN betavoltaics energy converters. 31st IEEE Photovoltaics Specialist Conference, Orlando, FL, 2005 Jan 3.

16. Li F, Gao X, Yuan Y, Yuan J, Lu M. GaN PIN betavoltaic nuclear batteries. Science China Technological Sciences: Nuclear Sci and Technology. 2014;57(1):25–28.

17. Cheng Z, Haisheng S, Li Y, Chen X. The design optimization for GaN-based betavoltaic microbattery. In: 2010 IEEE 5th International Conference on Nan/Micro Engineered and Molecular Systems, 2010.

18. Litz M. Monte carlo evaluation of tritium beta spectrum energy deposition in gallium nitride (GaN) direct energy conversion devices. Adelphi (MD): Army Research Laboratory (US); 2014 Sep. Report No.: ARL-TR-7082.

19. Wang G, Li H, Lei Y, Zhao W, Yang Y, Luo S. Demonstration of Pm-147 GaN betavoltaic cells. Nuclear Sci and Techniques. 2014;25(2).

20. Cross WG, Ing H, Freedman N. A short atlas of beta-ray spectra. Phys Med Biol. 1983;28(11):1251–1260.

21. Khan MRA. Design and characterization of p-i-n devices for betavoltaic microbatteries on gallium nitride. University of Maryland, Electrical and Computer Engineering Department, Masters of Science in Electrical Engineering 2015, College Park, Maryland, 2015 Sep 18.

22. Ray II. WB, Litz MS, Russo JA. Modeling and simulation of a GaN betavoltaic energy converter. Adelphi (MD): Army Research Laboatory (US); 2016. Report No.: ARL-TR-7675.

23. Lu M, Zhang G, Fu K, Yu G, Su D, Hu J. Gallium nitride schottky betavoltaic nuclear batteries. Energy Conversion and Management. 2011;52(4):1955–1958.

24. Cheng Z, San H, Chen X, Liu B, Feng Z. Demonstration of a high open-circuit voltage GaN betavoltaic microbattery. Chinese Phys Let. 2011;28(7).

25. Cheng Z, Zhao Z, San H, Chen X. Demonstration of a GaN betavoltaic microbattery. In: 2011 6th IEEE International Conference on Nano/Micro Engineered and Molecular Systems, 2011.

26. Tang X, Liu Y, Ding D, Chen D. Optimization design of GaN betavoltaic microbattery. Sci China Technol Sci. 2012;55(3):659–664.

27. San H, Yao S, Wang X, Cheng Z, Chen X. Design and simulation of GaN based Schottky betavoltaic nuclear microbattery. Appl Rad and Isotopes. 2013;80:17–22.

28. Liu Y, Tang X, Xu Z, Hong L, Wang H, Liu M, Chen D. Influences of planar source thickness on betavoltaics with different semiconductors. J Radioanalyt and Nuclear Chem. 2015;304(2):517–525.

29. Munson C, Arif M, Streque J, Belahsene S, Martinez A, Ramdane A, El Gmili Y, Salvestrini J, Voss P, Ougazzaden A. Model of Ni-63 battery with realistic PIN structure. J Appl Phys. 2015;118(10).

List of Symbols, Abbreviations, and Acronyms

2-D	2-dimensional
3-D	3-dimensional
Al	aluminum
Al_2O_3	sapphire
Au	gold
^{60}Co	cobalt-60
Cu	copper
DC	direct current
DEC	direct energy conversion
DIP	dual inline package
E_g	bandgap of semiconductor device
EHP	electron-hole pair
EPD	etching pit density
FF	fill factor
GaN	gallium nitride
^3H	tritium
HP	Hewlett-Packard
IDEC	indirect energy conversion
I_0, I_d	dark or leakage current
I_{sc}, I_g	short-circuit current
I-V	current-voltage curve
J_{sc}	short-circuit current density
MCNPX	Monte Carlo n-particle extended
MOCVD	metalorganic chemical vapor deposition
MPP	maximum power point
Ni	nickel

^{63}Ni	nickel-63
η	power conversion efficiency
Pm	promethium
^{147}Pm	promethium-147
R_{sh}	shunt resistance
S_e	output power density
Si	silicon
SiC	silicon carbide
Ti	titanium
Ti^3H_x	titanium tritide
V_{oc}	open-circuit voltage
V_m	voltage of the maximal power point
ZnS	zinc sulfide

1 (PDF) DEFENSE TECHNICAL INFORMATION CTR DTIC OCA

2 (PDF) DIRECTOR US ARMY RESEARCH LAB RDRL CIO LL IMAL HRA MAIL & RECORDS MGMT

1 (PDF) GOVT PRINTG OFC A MALHOTRA

4 (PDF) DIRECTOR US ARMY RESEARCH LAB RDRL SED E
JOHNNY A RUSSO
WILLIAM RAY
MARC S LITZ
STEPHEN KELLEY